



Deposited via The University of Sheffield.

White Rose Research Online URL for this paper:

<https://eprints.whiterose.ac.uk/id/eprint/160190/>

Version: Accepted Version

Article:

Angelova, P.R., Choi, M.L., Berezhnov, A.V. et al. (2020) Alpha synuclein aggregation drives ferroptosis : an interplay of iron, calcium and lipid peroxidation. *Cell Death & Differentiation*, 27 (10). pp. 2781-2796. ISSN: 1350-9047

<https://doi.org/10.1038/s41418-020-0542-z>

© 2020 The Authors. This is an author-produced version of a paper subsequently published in *Cell Death and Differentiation*. Uploaded in accordance with the publisher's self-archiving policy.

Reuse

Items deposited in White Rose Research Online are protected by copyright, with all rights reserved unless indicated otherwise. They may be downloaded and/or printed for private study, or other acts as permitted by national copyright laws. The publisher or other rights holders may allow further reproduction and re-use of the full text version. This is indicated by the licence information on the White Rose Research Online record for the item.

Takedown

If you consider content in White Rose Research Online to be in breach of UK law, please notify us by emailing eprints@whiterose.ac.uk including the URL of the record and the reason for the withdrawal request.

1 **Title: Alpha synuclein aggregation drives ferroptosis: an interplay of iron, calcium and lipid**
2 **peroxidation**

3 **Plamena R. Angelova^{1#}, Minee L. Choi^{1,8#}, Alexey V. Berezhnov², Mathew H. Horrocks⁷, Craig D.**
4 **Hughes⁷, Suman De^{7,10}, Margarida Rodrigues^{7,10}, Ratsuda Yapom³, Daniel Little⁴, Karamjit S.**
5 **Dolt³, Tilo Kunath³, Michael J. Devine⁴, Paul Gissen⁴, Mikhail S. Shchepinov⁹, Sergiy Sylantyev^{1,5},**
6 **Evgeny V. Pavlov⁶, David Klenerman^{7,10}, Andrey Y. Abramov^{1,11*}, Sonia Gandhi^{1,8*}**

7 *¹UCL Institute of Neurology, Queen Square, London WC1N 3BG, UK; ²Institute of Cell Biophysics,*
8 *Russian Academy of Sciences, Pushchino, 142290, Russia; ³MRC Centre for Regenerative Medicine, The*
9 *University of Edinburgh, Edinburgh, UK; ⁴MRC Laboratory for Molecular Cell Biology, University*
10 *College London, Gower Street, London, UK; ⁵ University of Aberdeen, Rowett Institute, Ashgrove Rd*
11 *West, Aberdeen AB25 2ZD; ⁶College of Dentistry, New York University, New York, USA; ⁷Department of*
12 *Chemistry, University of Cambridge, Cambridge, UK; ⁸The Francis Crick Institute, London, UK; ⁹*
13 *Retrotope Inc., Los Altos, California 94022, United States; ¹⁰Dementia Research institute at University of*
14 *Cambridge, Cambridge, UK; ¹¹Orel State University, Orel, Russia*

15

16 [#] Equally contributing author.

17 ^{*} Joint senior authors.

18 To whom correspondence should be addressed: Andrey Y. Abramov or Sonia Gandhi, UCL Institute of
19 Neurology, Queen Square House, Queen Square, London, UK, WC1N 3BG,

20 Tel.: (+44) 203 448 4062; E-mail: a.abramov@ucl.ac.uk ; sonia.gandhi@ucl.ac.uk

21

22 **Keywords:** *alpha-synuclein, calcium signalling, synucleinopathy, Parkinson's disease, Ferroptosis, iPSC-*
23 *derived neurons, electrophysiology*

24

25 **Abstract**

26 Protein aggregation and abnormal lipid homeostasis are both implicated in neurodegeneration through
27 unknown mechanisms. Here we demonstrate that aggregate-membrane interaction is critical to induce a
28 form of cell death called ferroptosis. Importantly the aggregate-membrane interaction that drives

1 ferroptosis depends both on the conformational structure of the aggregate, as well as the oxidation state of
2 the lipid membrane. We generated human stem cell derived models of synucleinopathy, characterised by
3 the intracellular formation of α -synuclein aggregates that bind to membranes. In human iPSC derived
4 neurons with SNCA triplication, physiological concentrations of glutamate and dopamine induce
5 abnormal calcium signalling due to the incorporation of excess α -synuclein oligomers into membranes,
6 leading to altered membrane conductance and abnormal calcium influx. α -synuclein oligomers further
7 induce lipid peroxidation. Targeted inhibition of lipid peroxidation prevents the aggregate-membrane
8 interaction, abolishes aberrant calcium fluxes, and restores physiological calcium signalling. Inhibition of
9 lipid peroxidation, and reduction of iron dependent accumulation of free radicals, further prevents
10 oligomer induced toxicity in human neurons. In summary, we report that peroxidation of polyunsaturated
11 fatty acids underlies the incorporation of β -sheet rich aggregates into the membranes, and that
12 additionally induces neuronal death. This suggests a role for ferroptosis in Parkinson's disease, and
13 highlights a new mechanism by which lipid peroxidation causes cell death.

14

15 **Introduction**

16 Synucleinopathies are neurodegenerative diseases that are characterised by the abnormal aggregation of
17 the protein α -synuclein, and include Dementia with Lewy Body Disease, Parkinson's Disease (PD) and
18 Multiple System Atrophy (MSA) (1). Within this group of diseases, it is evident that α -synuclein
19 aggregation, or Lewy Body pathology, occurs in diverse cell groups including the enteric nervous system,
20 midbrain dopaminergic neurons, and cortical neurons (2-5). Genetic evidence shows that alteration in the
21 concentration or structure of α -synuclein causes the synucleinopathies, in particular PD. Missense
22 mutations, and duplications or triplications of the SNCA gene, lead to autosomal dominant PD (6-9) that
23 is indistinguishable from sporadic PD, apart from early onset and a more aggressive course. Variations in
24 the SNCA gene that lead to increased α -synuclein expression represent a genetic risk factor for sporadic
25 PD (10).

26 Compelling pathological and genetic data defines α -synuclein as the cause of synucleinopathies, and
27 raises the question of how aggregation induces cellular dysfunction and death. During aggregation, α -
28 synuclein transitions from an intrinsically disordered monomeric protein to form small soluble oligomers
29 with increasing β -sheet content, followed by protofibrils and insoluble fibrils. The soluble intermediate
30 oligomeric species of α -synuclein may be 'toxic' to cells, and the toxicity of certain oligomers of α -
31 synuclein may be attributed to specific structural characteristics that confer damaging properties (11). It is
32 well established that α -synuclein interacts with lipids in its monomeric form, where it may regulate

1 synaptic vesicle trafficking (12). Importantly, oligomers of high β -sheet content and exposed hydrophobic
2 residues also interact with lipids, and disrupt or damage membrane structure, resulting in aberrant ion
3 fluxes (13-15). We have also demonstrated that oligomeric species can generate reactive oxygen species
4 within the cell, and this leads to the oxidation of lipids in the plasmalemmal and mitochondrial
5 membranes, as well as oxidation of mitochondrial proteins (13, 16, 17). Oligomer induced oxidation
6 events open the mitochondrial permeability transition pore, leading to apoptosis (18). However, other
7 forms of cell death also exist, and death by ‘ferroptosis’ has emerged to describe cell toxicity driven by
8 the iron dependent accumulation of lipid peroxides (19).

9 In this study, we utilized two human stem cell derived models of synucleinopathy to investigate how
10 protein aggregation, calcium signalling, and redox biology interact to induce toxicity. We investigate (i)
11 the effect of cellular uptake of exogenously applied recombinant oligomers, in which we can control the
12 structure and concentration of the species and (ii) the effect of longer term endogenous increased
13 expression of α -synuclein from SNCA mutations, and therefore the consequence of endogenously
14 generated oligomeric species. α -synuclein aggregation occurs in human neurons, and these aggregates
15 deregulate physiological calcium signalling, an effect dependent on the interaction between aggregates
16 and membranes. Importantly modulation of the oxidation state of the lipids changes the membrane - α -
17 synuclein interactions, and cell viability, highlighting the cell death pathway, ferroptosis, in these models.

18

19 **Material and Methods**

20 *Human stem cell derived models*

21 *Human Induced Pluripotent Stem Cell (iPSC) culture*

22 iPSCs were derived from donors who had given signed informed consent for derivation of iPSC lines
23 from skin biopsies as part of the EU IMI-funded programme StemBANCC. All experimental protocols
24 had approval from the London - Hampstead Research Ethics Committee (ref: 13/LO/0171, IRAS project
25 ID: 100318) and R&D approval from the University College London Great Ormond Street Institute of
26 Child Health and Great Ormond Street Hospital Joint Research Office.

27 iPSC-derived cortical neurons from 3 SNCA triplication (SNCA x3) clones and 3 control clones were
28 generated using standard protocols, and all experiments were performed on a minimum of 3 independent
29 inductions. Experiments were repeated using the SNCA x3 clones, and an isogenic clone generated from
30 the same patient. iPSCs were generated from a patient with early onset autosomal dominant PD due to a
31 triplication of the SNCA gene (encoding α -synuclein) using viral transduction of OCT4, SOX2, KLF4
32 and c-MYC (20). SNCA x3 results in four copies of the SNCA gene, and a doubling of SNCA mRNA

1 and α -synuclein protein. CRISPR/Cas 9 nickase technology was employed to remove 2 SNCA alleles to
2 restore the SNCA gene dosage to 2 copies, whilst retaining the rest of the triplication locus (that is, the
3 isogenic control, (21). The isogenic cell line was generated from a *SNCA* x3 iPSC clone by CRISPR/Cas9
4 double nickase gene editing to knockout 2 *SNCA* alleles, reducing the allele dosage from 4 (in the
5 triplication cells) to 2 (normal). This method retains the rest of the triplication locus intact, and therefore
6 provides the ideal control for the effects of *SNCA* x3 alone.
7 iPSCs were cultured on Geltrex (Thermo-Fisher) in Essential 8 medium (Thermo-Fisher) and passaged
8 using 0.5 mM EDTA (Thermo-Fisher). Neural induction was performed through dual SMAD inhibition
9 using SB431542 (10 μ M, Tocris) and Dorsomorphin dihydrochloride (1 μ M Tocris) within N2B27 media
10 - DMEM;F12+ glutamax, Neurobasal, B28, N2, Glutamax, Insulin, Non Essential Amino Acids, 2-
11 mercaptoethanol, Pen/strep- (modified from (22)). Cells were first passaged with Dispase (Thermo-Fisher,
12 1:2) at day 10 upon first appearance of the neuroepithelial sheet. Upon appearance of neural rosettes at
13 day 20 - 21, cells are passaged again with Dispase. Cells were passaged approximately 3 more times
14 before being used at day 70 - 90. All lines were mycoplasma tested (all negative) and performed with
15 STR profiling (all matched) by the Francis Crick Institute Cell service team.

16 *Human Embryonic Stem cells (ES) culture*

17 The hESC line was kindly provided by Dr. David Hay (University of Edinburgh), upon MRC Steering
18 Committee approval (ref. no. SCSC11-60). The line was established at the Centre for Stem Cell Biology
19 (University of Sheffield) under a license from the Human Fertilisation and Embryology Authority, and
20 has been validated to show the standard hESC characteristics including a normal karyotype. Briefly,
21 pCAG-SNCA-IRES-Venus or the control pCAG-IV were transfected into hES cells followed by
22 antibiotic selection to allow the generation of clones with stable expression of SNCA. Clones exhibiting
23 normal morphology, growth and differentiation behaviour were selected and characterised for SNCA
24 expression, and two clones with near normal levels of SNCA expression (here designated control) and
25 high levels of SNCA expression (designated as hES OE syn) were utilized for further studies.

26 For neural induction, hES cells were dissociated into single cells with Accutase (Gibco, Cat. no. A11105-
27 01) and plated on a Matrigel-coated 6-well plate in mTeSR1 medium. Cells were fed daily until they
28 reached 90% confluency or above. Neural induction started at day 0, when mTeSR1 was replaced with
29 hESC medium lacking FGF2, supplemented with 10 μ M SB431542 (Tocris) and 100 nM LDN-193189
30 (Stemgent). Cells were fed daily with this medium until day 4. From day 5 to day 11, SB431542 was
31 withdrawn and cells were fed every other day with a mixture of hESC medium and N2B27, which was
32 gradually added into culture medium from 25%, 50%, 75% and 100% at day 5, day 7, day 9 and day 11,

1 respectively. pCAG-SNCA-IRES-Venus or the control pCAG-IV were transfected into hES cells
2 followed by antibiotic selection to allow the generation of clones with stable expression of SNCA. Clones
3 exhibiting normal morphology, growth and differentiation behaviour were selected and characterised for
4 SNCA expression, and two clones with near normal levels of SNCA expression (here designated control)
5 and high levels of SNCA expression (designated as hES OE syn) were utilized for further studies.

6

7 ***Aggregation of α -synuclein***

8 Wild-type α -synuclein and A90C variant were purified from *Escherichia coli*. as previously described by
9 Hoyer *et al* (23). All α S aggregations (using labelled or unlabelled protein) were conducted in LoBind
10 microcentrifuge tubes (Eppendorf) to limit surface adsorption.

11 For the aggregation reactions of unlabeled recombinant α -synuclein, a 70 μ M solution of wild-type α -
12 synuclein in 25 mM Tris buffer with 100 mM NaCl pH 7.4 (supplemented with 0.01% NaN₃ to prevent
13 bacterial growth during aggregation) was incubated at 37°C with constant agitation at 200rpm (New
14 Brunswick Scientific Innova 43), during which time aliquots were taken.

15 For the aggregation reactions of labelled α -synuclein, the A90C variant of monomeric α S was labeled
16 with maleimide-linked Alexa Fluor 488 (AF488) or Alexa Fluor 594 (AF594) (Life Technologies) as
17 described previously (16, 24). The excess dye was removed by passing the labeled protein through a P10
18 desalting column containing Sephadex G25 matrix (GE Healthcare, Waukesha, WI). After elution, protein
19 concentration was determined using a nanodrop and the sample divided into aliquots, before being flash-
20 frozen in liquid nitrogen and stored at -80 °C. Each aliquot was only thawed once prior to use. AF488-
21 labelled and AF594-labelled monomeric α S were diluted in Tris buffer (same composition as mentioned
22 above) at a concentration of 70 μ M. For FRET experiments, AF488-labelled and AF594-labelled
23 monomeric α S were incubated together to a final concentration of 70 μ M. Similar to the aggregation of
24 unlabeled α S, the reaction was performed in the dark at 37 °C with constant agitation at 200 rpm (same
25 incubator as above) and aliquots were withdrawn at specific time points.

26 Different time points of unlabelled α -synuclein aggregation reaction were characterized using a highly
27 sensitive single-molecule method termed SAVE (Single Aggregate Visualisation by Enhancement)
28 imaging, which uses single-molecule fluorescence microscopy to detect the benzothiazole salt thioflavin-
29 T (ThT) see Sup Fig 1. Upon binding to β -sheet structures, ThT fluorescence increases allowing
30 individual aggregated species to be detected. From 2 h onwards, the number of diffraction limited
31 fluorescent puncta increases, which represents the emergence of oligomers and at later time points (> 24

1 h), fibrils as long as 5 μm are observed. For this study, we used time point 0h (no aggregates), 8h
2 (maximum number of oligomers without the presence of fibrils) and 24 h (16)(fibrils). The kinetics of
3 labelled α -synuclein reaction is different from the unlabelled and the time point that maximizes the
4 number of oligomers is around 29h and fibrils appear after 72h.

5

6 ***Deuteration of PUFAs***

7 Deuteration of PUFAs, Deuterated Poly-Unsaturated Fatty Acids (D-PUFAs) were prepared as described
8 previously (25) and used as free acids. Non-deuterated PUFAs were obtained from Sigma–Aldrich (99%;
9 St. Louis, MO, USA). Cells were pre-incubated with 10 μM D-PUFA in the culturing media for 48 hrs
10 prior to experiment and washed with HBSS before experiments.

11

12 ***Live Imaging (Fluorescence Measurements)***

13 Fluorescent indicators (fura-2 AM, Dihydroethidium, C11-BODIPY, SYTOX Green) were used to
14 measure $[\text{Ca}^{2+}]_i$, reactive oxygen species (ROS), and lipid peroxidation, and cell death respectively. The
15 fluorescent data was collected using a cooled camera device or a confocal microscope. For fluorescence
16 measurements with cooled camera device, data were obtained on an epifluorescence inverted microscope
17 equipped with a x 20 fluorite objective. For confocal microscopy, images were obtained using an either
18 Zeiss 710 or 880 (airy) vis CLSM equipped with a META detection system and a 40x oil immersion
19 objective. Illumination intensity was kept to a minimum (at 0.1 - 0.2 % of laser output) to avoid
20 phototoxicity and the pinhole set to give an optical slice of $\sim 2 \mu\text{m}$. All data presented were obtained from
21 at least 3 coverslips and 2 - 3 different induction.

22 For measurements of $[\text{Ca}^{2+}]_i$, cells were loaded for 30 min at room temperature with 5 μM Fura-2 AM
23 with 0.005% pluronic acid in a HEPES-buffered salt solution (HBSS) composed of (mM): 156 NaCl, 3
24 KCl, 2MgSO₄, 1.25 KH₂PO₄, 2 CaCl₂, 10 Glucose and 10 HEPES; pH adjusted to 7.35 with NaOH.
25 $[\text{Ca}^{2+}]_i$ was monitored in single cells using excitation light provided by a Xenon arc lamp, the beam
26 passing through monochromator centred sequentially at 340 and 380 nm (Cairn Research, Kent, UK).
27 Emitted fluorescence light was reflected through a 515 nm long-pass filter to a cooled CCD camera
28 (Retiga, QImaging, Canada). All imaging data was collected and analysed using software from Andor
29 (Belfast, UK). The Fura–2 data have not been calibrated in terms of $[\text{Ca}^{2+}]_i$ because of the uncertainty
30 arising from the use of different calibration techniques. For Dihydroethidium (Het) we generated ratios of

1 the oxidised form (ethidium) excited at 530 nm and measured using a 560 nm longpass filter and the
2 reduced form with excitation at 380 nm, measured between 415 - 470nm.

3 To assess lipid peroxidation, cells were loaded with C11-BODIPY (581/591, 2 μ M, Molecular Probes) in
4 HEPES buffered HBSS for 20 min prior to imaging and then excited using the 488 and 565 nm laser and
5 fluorescence measured from 505 to 550 nm and above 580 nm (409 objective) using a confocal
6 microscopy. The intensely fluorescent C11-BODIPY 581/591 fluorophore is an intrinsically lipophilic
7 dye which results in accumulation within membranes. Upon oxidation of the polyunsaturated butadienyl
8 portion of the dye, there is a shift of the fluorescent emission peak from 590 nm to 510 nm, and it remains
9 lipophilic, thus reflecting lipid peroxidation in membranes.

10 For SYTOX green (Molecular Probes), cells were loaded with SYTOX green in HEPES buffered HBSS
11 for 15 min. High-throughput images were acquired using an Opera Phenix High-Content Screening
12 System (PerkinElmer). SYTOX green staining was imaged by 488 nm and 405 nm for Hoechst staining
13 nuclei. Total 17-22 fields of images were taken per wells. Then the percentage of cell death was
14 quantified by the ratio between the number of Sytox green positive cells and the total number of Hoechst
15 expressing cells per image using a Columbus StudioTM Cell Analysis Software.

16 To visualise cytoplasmic membrane, cells were washed with HBSS and incubated with either CellMask
17 deep red Plasma membrane Stain (ThermoFisherScientific, 5 μ g/ml) for 5-10min or CellBriteTM Blue
18 (Biotium, 5 μ M) for 30min in HBSS and live-cell imaging was performed.

19

20 *Measuring α -synuclein aggregate induced Ca^{2+} influx*

21 To characterise aggregation in neurons derived from SNCA x3, lysates and media were collected from
22 both control and SNCA x3. Cells were lysed mechanically without using a lysis buffer. The lysates and
23 media were collected in an Eppendorf tube and centrifuged at 15000 rpm for 15 min. Supernatant was
24 collected in a fresh Eppendorf tube and kept in -80 until use.

25 For the membrane permeabilization assay, vesicles are prepared as previously described (26). Using this
26 assay, it has been previously shown α -synuclein oligomers disrupt and permeabilise membranes (27, 28).
27 Briefly, vesicles are synthesized using Phospholipids 16:0-18:1 PC and biotinylated lipids 18:1-12:0
28 Biotin PC (100:1) using freeze thaw method and mean diameter is 200 nm. Vesicles of oxidised lipid was
29 made using oxPAPC (Oxidized 1-palmitoyl-2-arachidonoyl-sn-glycero-3-phosphocholine) and 18:1-12:0
30 Biotin PC. Each vesicle is filled with 100 μ M Cal-520 dye and immobilised in PLL-g-PEG coated plasma

1 cleaned glass coverslips using biotin-neutravidin linkage. The surrounding of the vesicles was filled with
2 Ca^{2+} buffer. 50 μL of sample was incubated with the vesicles for 15 minutes and Ca^{2+} influx was
3 quantitatively measured using a homebuilt Total Internal Reflection Fluorescence Microscope (TIRFM)
4 based on an inverted Nikon Ti-2 microscope. 488 nm laser was focused back-focal plane of the 100X,
5 1.49NA oil immersion objective lens used to excite the Cal-520 dye. The fluorescence signal was
6 collected by the same objective and magnified 1.5 times. Then the emission light was passed through a
7 long pass filter (BLP01-488R-25) and a band pass filter (FF01-520/44-25) before imaged in EmCCD
8 camera. To check if the aggregate present in SNCA x3 media and lysates are composed of α -synuclein,
9 we have used previously reported method to determine the composition of the aggregates (29, 30). Media
10 was incubated with Anti-Alpha-synuclein (phospho S129) antibody (Abcam ab51253), for 30 min and
11 then added to the coverslips containing dye filled vesicles. Statistical significance test was performed
12 using two sample unpaired t-test.

13

14 ***Electrophysiology***

15 *Single-channel electrophysiology in living neurons*

16 Patch-clamp recordings of α -synuclein channels overexpressed in iPSC-derived neurons were performed
17 in perfusion solution containing: 124 mM NaCl, 3 mM KCl, 1 mM CaCl_2 , 3 mM MgCl_2 , 26 mM
18 NaHCO_3 , 1.25 mM NaH_2PO_4 , 10 mM D-glucose, 2 mM CaCl_2 , 2mM MgCl_2 , bubbled with 95:5 O_2/CO_2
19 (pH 7.4). To isolate response of α -synuclein channels we added to external solution 50 μM D-APV, 10
20 μM NBQX, 100 μM picrotoxin and 1 μM strychnine. Outside-out patches were excised from cell soma
21 with 5-6 MOhm borosilicate glass pipette and held at -70 mV membrane potential. Intrapipette solution
22 contained 117.5 mM Cs-gluconate, 17.5 mM CsCl, 10 mM KOH-HEPES, 10 mM BAPTA, 8 mM NaCl,
23 5 mM QX-314, 2 mM Mg-ATP, 0.3 mM GTP. As a control, we performed recordings from outside-out
24 patches pulled from iPSC-derived neurons received from healthy volunteers.

25 Recordings were performed at 33-35 $^\circ\text{C}$ using Multiclamp-700B amplifier, in whole-cell mode; signals
26 were digitized at 10 kHz. Recording electrodes were pulled from the thick-wall borosilicate glass
27 capillaries and fire-polished to 5-7 MOhm resistance.

28 In human stem cell derived neurons, to calculate and visualise amplitude characteristic for ion channel
29 openings, we constructed all-points histograms with 0.1 pA bin, and fitted them with a double-Gaussian
30 function:

$$F = \frac{p_1 e^{-\frac{(n-m_1)^2}{2\sigma_1^2}}}{\sigma_1 \sqrt{2\pi}} + \frac{p_2 e^{-\frac{(n-m_2)^2}{2\sigma_2^2}}}{\sigma_2 \sqrt{2\pi}},$$

where m_1 and m_2 are the mode values of Gaussians, σ_1 and σ_2 are the standard deviations of corresponding modes, n is the value of electrical current, and p_1 and p_2 are the fitting constants.

With this approach the mode value for the open state was fitted as 2.17 pA.

Channel activity in liposomes

Giant liposomes were prepared as described previously (31). Briefly, liposomes were formed by sonication of lipid (type IV-S soybean L- -phosphatidylcholine; Sigma-Aldrich) in water. Liposomes (600 μ g lipid) were mixed with 5 mM Hepes, pH 7.4 (50 μ l volume) and with protein sample (5 μ l), and dotted on a glass slide. Samples were dehydrated (3 h) and rehydrated overnight with 150 mM KCl, 5 mM Hepes, pH 7.4, at 4 C. Patch-clamp procedures and analysis used were described previously (18). membrane patches were excised from liposomes after formation of a giga-seal using micropipettes with \sim 0.4- μ m diameter tips and resistances of 10–20 Ω M at room temperature. Voltage clamp was performed with the excised configuration of the patch-clamp technique using an Elements eONE patch clamp amplifier in the inside-out mode. Voltages are reported as pipette potentials. Current traces were processed using pCLAMP software. Traces for figure and all points histograms were prepared using Origin 9.

ELISA assay

To measure the concentration of oligomeric α -synuclein, cell lysates were mechanically from CTRL and SNCA x3 neurons. α -synuclein oligomer was analysed using Human α -synuclein, alpha (non A4 component of amyloid precursor) oligomer (SNCA oligomer) ELISA kit (CSB-E18033h, Generon) and then normalized by total protein per well using Pierce BCA Protein Assay Kit (23225, ThermoFisherScientific).

Aptamer staining

1 Cells were permeabilized with 0.25 Triton X 100 and blocked with 10% Normal Goat Serum for 20 min
2 followed by another 3 hrs with 0.1% Triton X -100 and 10% Normal Goat Serum. Then cells were
3 incubated overnight with 0.5uM ATTO 425 labelled Aptamer (32). Cells were washed three times with
4 PBS and imaged.

5

6 ***Immunohistochemistry***

7 Cells (cultured in ibidi chamber) were fixed in 4% paraformaldehyde and permeabilized with 0.2%
8 Triton-100. 5% BSA was used to block non-specific binding. Cells were incubated with primary antibody
9 for 1hr at room temperature and washed three times with 5% BSA. Cells were incubated with secondary
10 antibody (see SFigure 1 for antibody lists) for 1hr at room temperature. Cells were imaged with PBS after
11 three times wash. Hoechst was added in the second wash if required.

12

13 ***Statistical analysis***

14 Statistical analysis (unpaired two sample t-test or one-way ANOVA, P value is set at 0.05) and curve
15 fitting were performed using Origin 2018 (Microcal Software Inc., Northampton, MA) software. Results
16 are expressed as means \pm standard error of the mean (S.E.M.). N = number of inductions and n= number
17 of cells, if not stated otherwise. Sample sizes for experiments were selected to capture adequate technical
18 variation (number of cells; numbers of fields of view; number of coverslips) and biological variation
19 (numbers of independent inductions; numbers of clones/patient line). Variance within each group was
20 estimated using a F-statistics (sum of squares). All experiments were repeated minimum three times. All
21 experiments were performed in a count balance manner and data was collected and analysed without bias.

22

23 **Results**

24 ***Human iPS derived neurons with increased α -synuclein exhibit abnormal calcium signalling.***

25 Differentiation of control iPSCs (control, or CTRL), SNCA triplication iPSCs (SNCA x3), and isogenic
26 control iPSCs, into cortical neurons was performed. The SNCA x3 mutation is a gene triplication, leading
27 to a doubling of α -synuclein protein expression (20). We generated enriched populations of neurons from
28 both control and SNCA x3 mutant lines, with a small proportion of glial-like cells (Figure 1 A, B).

1 Immunocytochemistry (α -synuclein Ab MJFR1, Abcam), demonstrated elevated α -synuclein protein
2 expression in SNCA x3 cells (SFigure 2 Aa & b).

3 We investigated whether physiological calcium responses are altered by increased expression of α -
4 synuclein. We stimulated iPSC-derived neurons with physiological concentrations of glutamate (5 μ M)
5 and KCl (50 mM) which induces opening of potential-sensitive Ca^{2+} channels that are specific for
6 neurons. We then stimulated a calcium signal with 100 μ M ATP which induces activation of P2Y
7 receptors (33). There is no significant difference in the proportion of cells responding to either glutamate
8 (neurons) or ATP stimuli (glia-like) in CTRL, SNCA x3 and Iso-CTRL (Figure 1 Ca & b). Stimulation of
9 neurons with 5 μ M glutamate induces a significantly higher signal in SNCA x3 cells compared to both
10 isogenic control and healthy control cells (CTRL: 0.65 ± 0.04 , $n=96$, SNCA x3: 1.2 ± 0.1 , $n=99$; $p < 0.001$,
11 Figure 1 Cc, Da & d). The physiological $[\text{Ca}^{2+}]_c$ response to 50 mM KCl was also higher in SNCA x3
12 iPSC-derived neurons (0.29 ± 0.01 , $n=101$) when compared to control neurons (1.01 ± 0.039 , $n=114$;
13 $p < 0.001$; Figure 1 Db & d). Stimulation with 100 μ M ATP leads to an increase in $[\text{Ca}^{2+}]_c$ in glial-like
14 cells, but not in neurons. This $[\text{Ca}^{2+}]_c$ response was significantly lower in glial-like cells with SNCA x3
15 when compared to control cells (0.49 ± 0.03 , $n=68$ in CTRL; $p < 0.001$; Figure 1 Dc & d). We also detected
16 an impairment of intracellular calcium homeostasis in SNCA x3 showing re-distribution of Ca^{2+} stores,
17 and depletion of ER calcium, and increase in mitochondrial calcium (SFigure 3).

18 One of the major characteristics of mature neurons is their spontaneous calcium activity. Spontaneous
19 calcium transients were observed in all iPSC-derived cortical neurons (Figure 1 Ea), with no significant
20 difference in the amplitude of these transients (Figure 1 Eb) between CTRL and SNCA x3.

21

22 ***Increased expression of α -synuclein in a hES model demonstrates altered calcium signalling.***

23 To test the effect specifically of SNCA expression in neurons, we utilized a model of transgenic human
24 stem cell derived neurons engineered to express SNCA at control or high levels (18), on an isogenic
25 background. Both control and SNCA o/e cells displayed a native-like membrane potential of 61 ± 5 mV
26 ($n=4$), characteristic for neurons, and generated action potentials of classical shape in response to current
27 injection. Action potentials in SNCA o/e cells were generated with significantly lower frequency: 4.2 ± 1.3
28 Hz vs. 18.7 ± 3.4 Hz in control, $P < 0.01$, $n=4, 7$, Student's t-test. 1 μ M of Tetrodotoxin (TTX) added into
29 the perfusion solution fully suppressed action potential generation, revealing the presence of voltage-
30 gated sodium channels in the tested cells (SFigure 4 Aa & b).

1 To test the calcium response to physiological stimuli, we applied glutamate (10 μ M) which induces a
2 typical calcium transient in control neurons, and SNCA o/e (SFigure 4 Ba & d, CTRL; n=47 cells,
3 SNCAx3; n=32 cells). In agreement with previous results, glutamate-induced calcium signal in SNCA o/e
4 was significantly higher than those found in CTRL (signal rose to 1.3 \pm 0.24 Fura-2 ratio compared to
5 0.7 \pm 0.08 Fura-2 ratio, p<0.05). More than 60% cells demonstrated typical response to plasma membrane
6 depolarisation with opening of voltage-gated calcium channels (SFigure 4 Bc & d). Again, SNCA o/e
7 cells had significantly higher calcium responses to 50mM KCl (SFigure 4 Bc & d, CTRL; 0.92 \pm 0.1 Fura-
8 2 ratio, n=39, SNCAx3; compared to 0.61 \pm 0.08 Fura-2 ratio in control, n=38 cells; p<0.05).

9 Application of 100 μ M ATP stimulates calcium signalling via P2Y receptors, expressed predominantly in
10 astrocytes. Approximately 40% of cells in the field demonstrated a calcium response to application of
11 ATP, and SNCA o/e cells demonstrated a higher ATP-induced calcium signal than control cells (SFigure
12 4 Bb & d, CTRL; 1.21 \pm 2.2 Fura-2 ratio, n=37, SNCAx3; compared to control 0.97 \pm 0.07 Fura-2 ratio,
13 n=47 cells; p<0.05).

14

15 **Alpha-synuclein aggregates disrupt membranes and alter membrane conductance.**

16 We investigated how α -synuclein aggregates disrupt membranes and induce ion fluxes. Using a
17 ATTO425-labelled Aptamer that recognises aggregates of α -synuclein (32), we confirmed the increase in
18 aggregates in the SNCA x3 cells, demonstrated both by intensity, and area of cell occupied by aggregates.
19 (Figure 2 A). This aptamer, using super resolution microscopy (ADPAINT) has demonstrated an increase
20 in larger aggregates in SNCA x3 neurons (32). We performed an oligomer ELISA to measure the soluble
21 aggregates in the SNCA x3 and CTRL cell lysates (SFigure 5), and demonstrated a selective increase in
22 oligomers in the SNCA x3 neurons (SFigure 5 B).

23 Aggregates formed in the SNCA x3 cells, and secreted in the media, are capable of permeabilising
24 membranes, and inducing ion fluxes. Using a single vesicle assay, we demonstrated that application of
25 SNCAx3 lysates and media induced calcium influx across liposomes. This calcium influx was blocked
26 after incubation of SNCAx3 lysates and media (25x dilution) with Anti- α -synuclein (phospho S129)
27 antibody (see Figure 2 Ba for experimental paradigm). Therefore, both secreted oligomers in the
28 extracellular space of SNCA x3, as well as internally generated oligomers possess a structural
29 conformation that can interact with, and disrupt, membranes (Figure 2 Bb & c) to induce calcium fluxes.

30 To test the effect of increased endogenous α -synuclein on the membrane conductance of neurons, we
31 performed patch-clamp recordings from outside-out membrane patches in a voltage-clamp mode. To

1 isolate the response solely of channels formed by α -synuclein aggregates, we added to the external
2 solution 50 μ M D-APV, 10 μ M NBQX, 100 μ M picrotoxin and 1 μ M strychnine. We registered single-
3 channel openings in patches excised from iPSC-derived neurons with SNCA x3 (channel conductance
4 189 ± 26 pS, n=5) while no single-channel activity was observed in control neuronal cultures when a
5 similar cocktail of ion channel blockers was applied (Figure 2 Ca). However, we managed to detect
6 activity only in a small fraction of SNCA x3 neurons (Figure 2 Ca); five successful recordings out of 29
7 outside-out patches (each patch was pulled from a separate cell). To calculate the amplitude of the ion
8 channel opening, all point histograms were constructed and fitted to a double Gaussian function. The
9 mode value for the open state was fitted at 2.17 pA (Figure 2 Cb). This data suggests the presence of
10 channel formation on the plasmalemmal membrane of neurons with high levels of α -synuclein,
11 independent on any known ion channels.

12 We investigated the effect of α -syn aggregates on the ion permeability of membranes, using patch-clamp
13 of giant liposomes exposed to recombinant α -synuclein oligomers. We detected single channel activity
14 induced by oligomers of α -syn, but not monomers (Figure 2 Da & b), and these channels had multiple
15 conductance levels, with opening and partial inactivity to stable subconductance at a constant voltage,
16 followed by higher conductance states induced at -20mV.

17

18 ***Increased expression of α -synuclein leads to generation of reactive oxygen species and membrane*** 19 ***oxidation.***

20 We have reported that oligomeric α -synuclein drives the aberrant generation of intracellular superoxide
21 and hydrogen peroxide, and the depletion of antioxidants (17, 34). Basal superoxide production is
22 increased in the SNCA x3 iPSC-derived neurons (17) and addition of recombinant oligomers further
23 increased superoxide production (CTRL; 175 ± 11.9 %, N=4, $p < 0.0001$, SNCA x3; 158.3 % to $343.0 \pm$
24 37.3 %, N=4, $p < 0.0001$, Figure 3 A). Consistently, hES cells with SNCA o/e also produce abnormal
25 levels of superoxide (SFigure 6). SNCA x3 iPSC-derived neurons also exhibit an increase in basal lipid
26 peroxidation from 0.161 ± 0.004 to 0.241 ± 0.007 , both N=4, $p < 0.0001$; addition of oligomers to control
27 cells increased lipid peroxidation to 0.456 ± 0.003 , N=4, $p < 0.0001$; similarly, addition of oligomers to
28 SNCA x3 increased lipid peroxidation to 0.408 ± 0.005 , N=4, $p < 0.0001$ (Figure 3 B).

29 Isotopic reinforced polyunsaturated fatty acids (D-PUFAs) incorporate into lipid membranes and render
30 them resistant to the ROS initiated chain reaction of lipid peroxidation. We pre-treated cells with 10 μ M
31 deuterated Linolenic acid (D4-Lnn), which prevented oligomer induced lipid peroxidation, and restored
32 basal levels of lipid peroxidation in the SNCA x3 cells (Fig 3 B). Therefore, recombinant oligomers, as

1 well as oligomers generated in the SNCA x3 cells, induce oxidation of PUFAs, which can be modulated
2 by the use of deuterated species.

3

4 ***Lipid peroxidation influences the physical interaction of aggregates and membranes.***

5 α -synuclein- membrane interactions in cells are transient and difficult to capture. Membrane binding to
6 the plasma membrane is a prerequisite prior to internalization of α -synuclein into the cell (35). Labelled
7 oligomers (oligomers generated from AF488 monomeric α -synuclein) were applied to cells loaded with
8 either a cell mask dye, or a membrane dye. Internalization of fluorescently labelled monomer and
9 oligomer is demonstrated in figure 3 Ca and SFigure 7 Aa. Vitamin E is a tocopherol that inhibits lipid
10 peroxidation by scavenging lipid peroxy radicals. We pre-incubated cells with Trolox, a water soluble
11 analogue of α -tocopherol which is able to incorporate into both water and lipid compartments, reduced
12 the α -synuclein accumulation in the cell (as demonstrated by reduced AF488 area/cell, Figure 3 Cb and
13 SFigure 7Ab).

14 Next, we tested the effect of membrane oxidation on insertion of aggregates into membranes utilizing the
15 membrane Permeabilization assay (described in Figure 2 Ca). Using vesicles generated from oxidized
16 lipids, there is higher calcium influx on exposure to the same concentration of α -synuclein oligomers,
17 compared to control lipid vesicle (Figure 3 D).

18 Together, this data suggests that under conditions of membrane oxidation, there is an enhanced membrane
19 binding of oligomers of α -synuclein, allowing ion fluxes across the membrane, as well as entry into the
20 cell. This interaction is reduced in cells with non-oxidized membranes.

21

22 ***Lipid peroxidation drives α -synuclein induced abnormal calcium signaling.***

23 Next we tested whether the α -synuclein induced calcium signaling is affected by lipid peroxidation. We
24 demonstrated abnormal glutamate induced calcium signaling in SNCA x3 neurons (Figure 4Ab & Bb).
25 Pre-incubation of cells for 24 hours with D4-Lnn restored the glutamate-induced calcium signaling back
26 to control levels (from 2.50 ± 0.27 , N=7, n=100, Figure 4 Ab & Da to 1.43 ± 0.25 , n=7, N=7, p=0.0113,
27 Figure 4 Ac & Da after the use of D4-Lnn). Pre-incubation of cells with D4-Lnn interestingly abolished
28 the KCL-induced opening of voltage-dependent calcium channels (from 1.65 ± 0.22 , N=9, n=114, Figure
29 4 Ab & Db to 0.30 ± 0.09 , N=5, n=165, p=0.0009, Figure 4 Ab & c, Db). ATP-induced calcium signal is
30 significantly smaller in the SNCA x3 cells compared to control (CTRL: 1.92 ± 0.27 , N=4, n=165, SNCA

1 x3: 0.75 ± 0.11 , N=4, n=114, p=0.0062, Figure 4 Ba & c). This was also restored by the pre-incubation of
2 D4-Lnn (1.70 ± 0.30 , N=4, n=120, p=0.0251, Figure 4 Bc & Dc).

3 We previously showed that dopamine induces calcium signaling through dopamine receptor independent
4 mechanisms (36, 37), and this includes (i) the opening of voltage dependent calcium channels following
5 dopamine uptake and depolarization of the plasmalemmal membrane and (ii) dopamine induced lipid
6 peroxidation and activation of phospholipase C and release of calcium from ER stores. Application of two
7 stimuli of dopamine induces a typical calcium response in control cells (37). However, SNCA x3 cells
8 exhibited a significantly higher calcium response to the second stimulus of dopamine compared to control
9 cells (SNCA x3: from 0.61 ± 0.09 , n=160, N=8, n=160 to 1.89 ± 0.21 , N=6, n=136, p=0.0001; Figure 4
10 Ca & b). The calcium response to dopamine in SNCA x3 was fully abolished when cells were pre-treated
11 with D4-Lnn (0.16 ± 0.08 , N=4, n=148, p=0.0002; Figure 4 C & c, Dd). Complete prevention of the
12 dopamine induced calcium response by D-PUFAs is likely to be due to blockade of both insertion of
13 channels into the membranes (in keeping with depolarizing stimuli), as well as blockade of the PLC/IP3
14 response. This data suggests that the incorporation of α -synuclein as a channel into the plasma membrane
15 occurs when the PUFAs in membranes have undergone lipid peroxidation. Non-oxidisable PUFAs lead to
16 membranes that are resistant to the insertion of oligomers and their channel-forming activity, and do not
17 demonstrate glutamate/dopamine induced calcium deregulation.

18

19 ***Oligomer-induced toxicity is dependent on iron and lipid peroxidation.***

20 SNCA x3 cells exhibit reduced cell viability compared to CTRL over time in culture, shown in Figure 5
21 Aa-b. We tested the sensitivity to ferroptosis of our iPSC derived synucleinopathy model using the
22 ferroptosis inducer, erastin, and we show that erastin induces a dose dependent increase in cell death,
23 shown in Figure 5 B. Oligomer-induced oxidative stress is dependent on transition metal ions (17). We
24 tested the effects of metal ion chelator (Desferoxamine, DFO), inhibitor of lipid peroxidation (D4-Lnn),
25 and a ferroptosis inhibitor (Ferrostatin-1) on cell death in synucleinopathy (38). Application of oligomers
26 but not monomers, induced cell death in control (Figure 5 Ca & b) neurons and SNCA x3 (Figure 5 Ca &
27 c) neurons. Application of three different ferroptosis inhibitors, deuterated PUFAs, iron chelator
28 desferrioxamine (DFO, Sigma), and ferrostatin-1 (Ferr-1, Sigma, Cat No. SML0583) each significantly
29 reduced oligomer induced cell death back to basal levels in control cells (Figure 5 Ca & b) and in SNCA
30 x3 cells (Figure 5 Ca & c). Taken together this data suggests that α -synuclein aggregates may induce
31 ferroptosis, and that inhibitors of ferroptosis prevent α -synuclein-induced cell death, and inducers of
32 ferroptosis exacerbate cell death.

1

2 **Discussion**

3 Ferroptosis (39) describes a form of non-apoptotic regulated cell death occurring as a consequence of
4 iron-dependent accumulation of lethal lipid peroxidation. Ferroptosis is characterized by cell swelling
5 (oncosis), altered mitochondrial morphology (40), and unique features of lipid peroxidation with
6 preferential oxidation of phosphatidylethanolamine (41). Suppression of the formation of oxidized lipids
7 halts cell death. The downstream pathways whereby lipid peroxidation leads to cell dysfunction or death
8 are not fully established, but are proposed to include loss of membrane integrity, opening of pores and
9 loss of ionic homeostasis, formation of free radicals that inactivates membrane embedded proteins
10 required for cell viability (42). The major criteria for determining ferroptosis are the ability to suppress
11 death by iron chelators, lipophilic antioxidants, inhibition of lipid peroxidation, and depletion of lipid
12 peroxidation.

13 In neurodegeneration (43), a number of ferroptosis features are commonly reported, in particular
14 depletion of glutathione, accumulation of lipid peroxidation products, excess extracellular glutamate,
15 decreased cortical GPX4, increased lipoxygenase (LOX) activity, protection from lipophilic antioxidant
16 vitamin E (in AD), protection from iron chelators (44), and protection from pioglitazone, an ACSL4
17 inhibitor (45). Additionally, brain iron levels rise in during aging and neurodegenerative disease, which
18 can be detected in living people (46) and in postmortem tissue. However, lipid peroxidation and
19 ferroptosis has not been previously investigated in synucleinopathy models of PD (47).

20 Here we study the complex intersection between protein aggregation, calcium deregulation and lipid
21 peroxidation. We have demonstrated that abnormal calcium fluxes, as well as abnormal intracellular
22 stores, is an important biological property of specific α -synuclein oligomers, when applied exogenously to
23 cell systems (13, 48). In this study, we demonstrate that increased endogenous levels of α -synuclein
24 oligomers, are associated with high cytosolic calcium influx in response to activation of glutamate
25 receptors or changes in plasmalemmal membrane potential. This could be attributable either to high
26 expression of potential-sensitive calcium channels or increased activation of glutamate receptors. Our
27 data suggests an increased presence of potential-sensitive channels on the plasmalemmal membrane of the
28 human neurons with high levels of oligomeric α -synuclein. Such channels are known to be formed by the
29 effect of α -synuclein beta-sheet rich oligomers on membranes (13). Notably, solution and solid-state
30 NMR methods have confirmed that the exogenously applied oligomers used in this study, result in
31 maximal membrane disruption by allowing the structured oligomer core to insert into the lipid bilayer and
32 disrupt the integrity (14). In our study, oligomers induce ion fluxes in the absence of the NMDA receptor

1 components in artificial systems (liposomes), and additionally oligomers induce channel formation in the
2 presence of NMDA blockade in outside out patches in cells, Taken together, this supports the hypothesis
3 that the α -synuclein oligomeric species alone are able to insert into membranes (in particular oxidized
4 membranes), upon depolarizing stimuli, leading to a voltage-dependent increase in cytosolic calcium
5 influx in response to glutamate, KCl and dopamine.

6 The second key feature is the ability for oligomeric α -synuclein, both when applied exogenously or when
7 generated endogenously, to induce the production of superoxide and hydrogen peroxide (17) and lipid
8 peroxidation (49). Notably, the mechanism of oligomer induced ROS production and lipid peroxidation is
9 iron dependent, and non-enzymatic, likely dependent on the Fenton reaction (18) (17). As protein
10 aggregates interact with, and disrupt, lipid membranes, we sought to modulate this interaction through
11 altering membrane properties by their oxidation state (50). Lipidomics has previously been used to
12 demonstrate that polyunsaturated fatty acids (PUFAs) are the most susceptible lipids in the course of
13 ferroptosis (41), and that preventing peroxidation by supplementing cells with PUFAs deuterated at the
14 susceptible bis-allylic carbon suppresses ferroptosis (51). Based on this, supplementation of media with
15 deuterated D4-linolenic acid has shown to prevent lipid peroxidation (49), and also to prevent ferroptosis
16 (51). We show that supplementation of the media with deuterated PUFAs is able to prevent oligomer
17 induced lipid peroxidation. We further demonstrated that in the absence of lipid peroxidation, the α -
18 synuclein-induced calcium dysregulation is also abolished, and physiological calcium signaling is
19 restored. This effect is true for glutamate-induced, KCL-induced and also dopamine-induced calcium
20 signaling which induces both a calcium influx (36), as well as generates ROS (37). We therefore
21 confirmed that lipid peroxidation allows membranes to be more susceptible to aggregates inserting into
22 them and disruption of ion fluxes. Stabilization of the oxidation state of the membrane prevents additional
23 oligomeric channel insertion, and reduces ion fluxes across the membrane. Our hypothesis is that the
24 oxidation state of the membrane confers its susceptibility to a physical and functional interaction with
25 beta sheet rich oligomeric proteins. It is possible that oxidized lipids recruit more oligomers to the
26 membrane, or that any individual rare oligomer event results in greater disruption of the membrane and
27 more calcium influx, and it is challenging to distinguish these two possibilities (52).

28 Iron chelators, d-PUFAs, and ferrostatin were all able to suppress cell death induced by toxic oligomeric
29 α -synuclein, or by dopamine in neurons. Inhibition of toxicity using reduction of iron, suppression of lipid
30 peroxidation, and ferrostatin meets the basic criteria set out for the definition of ferroptosis (53), and
31 therefore we raise the hypothesis that α -synuclein may contribute to cell death by this pathway, while
32 recognizing that other forms of apoptosis and necrosis also co-exist. The co-dependence of protein

1 aggregation, membrane damage and oxidative stress in ferroptosis in neurodegeneration may underlie
2 why models based on a single factor alone (eg GPX4 deletion) do not exhibit neurodegeneration (54).

3 Cellular aging, dopamine and α -synuclein oligomers place the cell in a state of aberrant ROS production
4 and glutathione depletion, resulting in oxidative stress with lipid peroxidation. Oxidation of specific
5 PUFAs, leads to the insertion of α -synuclein oligomers into the membrane forming channels that open in
6 response to depolarization of the plasma membrane. This renders neurons vulnerable to physiological
7 calcium signaling and exposes them to high levels of cytosolic calcium fluxes that may cause
8 excitotoxicity and cell death. At least part of the α -synuclein aggregate-induced cell death is related to
9 ferroptosis in which the iron dependent accumulation of lipid peroxidation plays an important role in the
10 demise of neurons. Whilst in cellular models, targeting lipid peroxidation specifically using deuterated
11 PUFAs, is a useful tool to demonstrate the contribution of lipid oxidation to calcium fluxes, its direct
12 application to patients may be hindered by the important physiological roles that lipid oxidation also plays
13 in neuronal function. Nonetheless, modulation of lipid peroxidation or ferroptosis may represent new
14 potential therapeutic approaches for Parkinson's disease.

15

16 **Acknowledgments**

17 This work was supported by the Wellcome/MRC Parkinson's Disease Consortium grant (grant number
18 WT089698), the Leverhulme Trust and the National Institute of Health Research University College
19 London Hospitals Biomedical Research Centre. SG was supported by Wellcome, and is an MRC Senior
20 Clinical Fellow. The study was funded additionally by RFBR, project number 20-34-70074. M Schepinov
21 is employed by Retrotope Inc. This work was supported by the grant of the Russian Federation
22 Government no. 075-15-2019-1877.

23

24 **Conflict of Interest**

25 M Schepinov is employed by Retrotope Inc. There is no other conflict of interest.

26

27 **References**

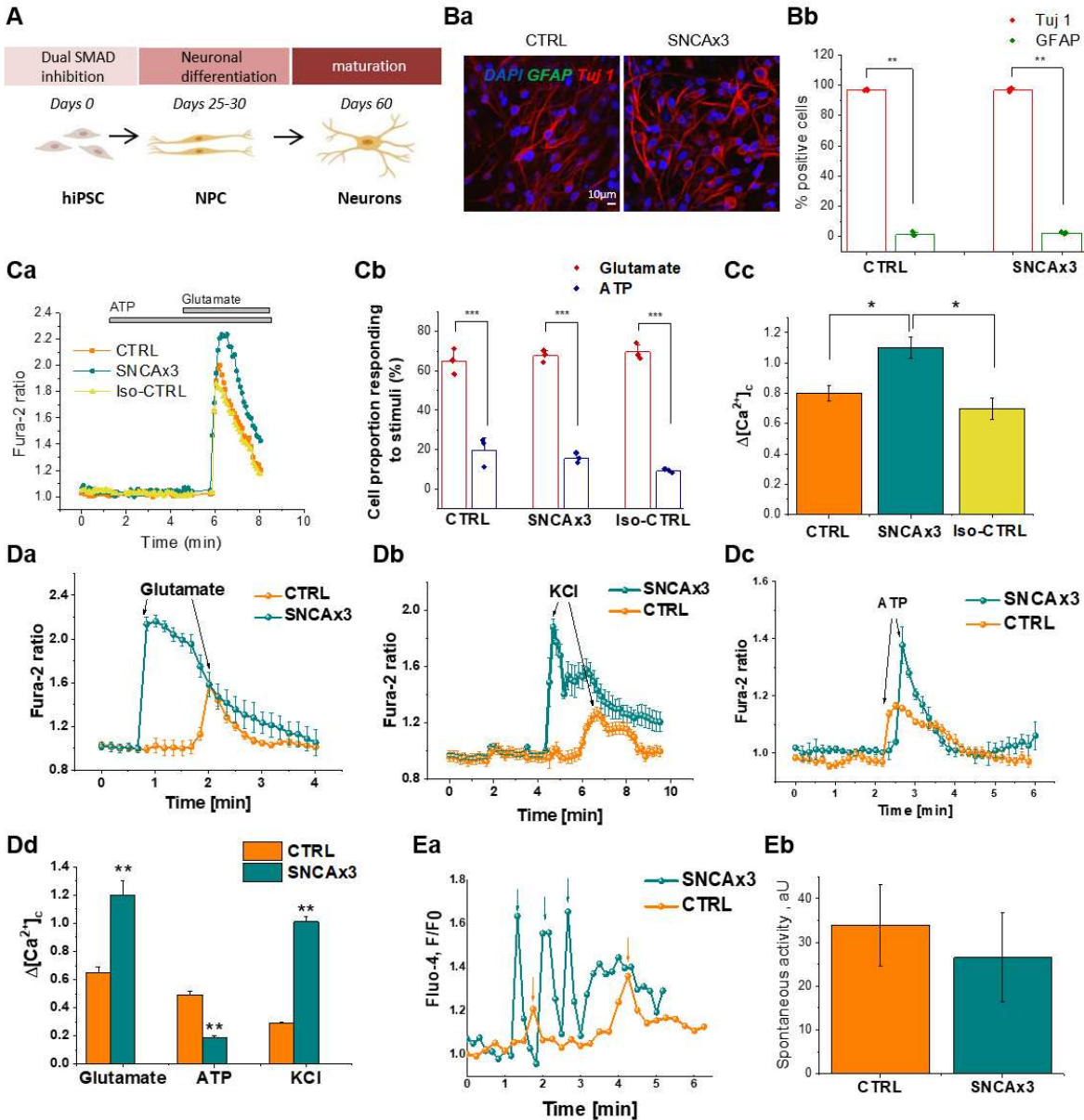
28 1. Goedert M, Jakes R, Spillantini MG. The Synucleinopathies: Twenty Years On. *Journal*
29 *of Parkinson's disease*. 2017;7(s1):S51-s69.

- 1 2. Arai K, Kato N, Kashiwado K, Hattori T. Pure autonomic failure in association with
2 human alpha-synucleinopathy. *Neuroscience letters*. 2000;296(2-3):171-3.
- 3 3. Lippa CF, Fujiwara H, Mann DM, Giasson B, Baba M, Schmidt ML, et al. Lewy bodies
4 contain altered alpha-synuclein in brains of many familial Alzheimer's disease patients with
5 mutations in presenilin and amyloid precursor protein genes. *The American journal of pathology*.
6 1998;153(5):1365-70.
- 7 4. Spillantini MG, Crowther RA, Jakes R, Hasegawa M, Goedert M. alpha-Synuclein in
8 filamentous inclusions of Lewy bodies from Parkinson's disease and dementia with lewy bodies.
9 *Proceedings of the National Academy of Sciences of the United States of America*.
10 1998;95(11):6469-73.
- 11 5. Yan F, Chen Y, Li M, Wang Y, Zhang W, Chen X, et al. Gastrointestinal nervous system
12 alpha-synuclein as a potential biomarker of Parkinson disease. *Medicine*. 2018;97(28):e11337.
- 13 6. Chartier-Harlin MC, Kachergus J, Roumier C, Mouroux V, Douay X, Lincoln S, et al.
14 Alpha-synuclein locus duplication as a cause of familial Parkinson's disease. *Lancet*.
15 2004;364(9440):1167-9.
- 16 7. Kruger R, Kuhn W, Muller T, Woitalla D, Graeber M, Kosel S, et al. Ala30Pro mutation in
17 the gene encoding alpha-synuclein in Parkinson's disease. *Nat Genet*. 1998;18(2):106-8.
- 18 8. Polymeropoulos MH, Lavedan C, Leroy E, Ide SE, Dehejia A, Dutra A, et al. Mutation in
19 the alpha-synuclein gene identified in families with Parkinson's disease. *Science (New York,*
20 *NY)*. 1997;276(5321):2045-7.
- 21 9. Singleton AB, Farrer M, Johnson J, Singleton A, Hague S, Kachergus J, et al. alpha-
22 Synuclein locus triplication causes Parkinson's disease. *Science (New York, NY)*.
23 2003;302(5646):841.
- 24 10. Nalls MA, Pankratz N, Lill CM, Do CB, Hernandez DG, Saad M, et al. Large-scale meta-
25 analysis of genome-wide association data identifies six new risk loci for Parkinson's disease.
26 *Nat Genet*. 2014;46(9):989-93.
- 27 11. Choi ML, Gandhi S. Crucial role of protein oligomerization in the pathogenesis of
28 Alzheimer's and Parkinson's diseases. *The FEBS journal*. 2018;285(19):3631-44.
- 29 12. Alza NP, Iglesias Gonzalez PA, Conde MA, Uranga RM, Salvador GA. Lipids at the
30 Crossroad of alpha-Synuclein Function and Dysfunction: Biological and Pathological
31 Implications. *Frontiers in cellular neuroscience*. 2019;13:175.
- 32 13. Angelova PR, Ludtmann MH, Horrocks MH, Negoda A, Cremades N, Klenerman D, et
33 al. Ca²⁺ is a key factor in alpha-synuclein-induced neurotoxicity. *Journal of cell science*.
34 2016;129(9):1792-801.
- 35 14. Fusco G, Chen SW, Williamson PTF, Cascella R, Perni M, Jarvis JA, et al. Structural
36 basis of membrane disruption and cellular toxicity by alpha-synuclein oligomers. *Science (New*
37 *York, NY)*. 2017;358(6369):1440-3.
- 38 15. Zakharov SD, Hulleman JD, Dutseva EA, Antonenko YN, Rochet JC, Cramer WA.
39 Helical alpha-synuclein forms highly conductive ion channels. *Biochemistry*. 2007;46(50):14369-
40 79.
- 41 16. Cremades N, Cohen SI, Deas E, Abramov AY, Chen AY, Orte A, et al. Direct
42 observation of the interconversion of normal and toxic forms of alpha-synuclein. *Cell*.
43 2012;149(5):1048-59.
- 44 17. Deas E, Cremades N, Angelova PR, Ludtmann MH, Yao Z, Chen S, et al. Alpha-
45 Synuclein Oligomers Interact with Metal Ions to Induce Oxidative Stress and Neuronal Death in
46 Parkinson's Disease. *Antioxidants & redox signaling*. 2016;24(7):376-91.
- 47 18. Ludtmann MHR, Angelova PR, Horrocks MH, Choi ML, Rodrigues M, Baev AY, et al.
48 alpha-synuclein oligomers interact with ATP synthase and open the permeability transition pore
49 in Parkinson's disease. *Nat Commun*. 2018;9(1):2293.
- 50 19. Conrad M, Kagan VE, Bayir H, Pagnussat GC, Head B, Traber MG, et al. Regulation of
51 lipid peroxidation and ferroptosis in diverse species. *Genes Dev*. 2018;32(9-10):602-19.

- 1 20. Devine MJ, Ryten M, Vodicka P, Thomson AJ, Burdon T, Houlden H, et al. Parkinson's
2 disease induced pluripotent stem cells with triplication of the alpha-synuclein locus. *Nat*
3 *Commun.* 2011;2:440.
- 4 21. Chen Y, Dolt KS, Kriek M, Baker T, Downey P, Drummond NJ, et al. Engineering
5 synucleinopathy-resistant human dopaminergic neurons by CRISPR-mediated deletion of the
6 SNCA gene. *Eur J Neurosci.* 2019;49(4):510-24.
- 7 22. Shi Y, Kirwan P, Livesey FJ. Directed differentiation of human pluripotent stem cells to
8 cerebral cortex neurons and neural networks. *Nature protocols.* 2012;7(10):1836-46.
- 9 23. Hoyer W, Antony T, Cherny D, Heim G, Jovin TM, Subramaniam V. Dependence of
10 alpha-synuclein aggregate morphology on solution conditions. *Journal of molecular biology.*
11 2002;322(2):383-93.
- 12 24. Ilijina M, Garcia GA, Horrocks MH, Tosatto L, Choi ML, Ganzinger KA, et al. Kinetic
13 model of the aggregation of alpha-synuclein provides insights into prion-like spreading.
14 *Proceedings of the National Academy of Sciences of the United States of America.*
15 2016;113(9):E1206-15.
- 16 25. Hill S, Hirano K, Shmanai VV, Marbois BN, Vidovic D, Bekish AV, et al. Isotope-
17 reinforced polyunsaturated fatty acids protect yeast cells from oxidative stress. *Free radical*
18 *biology & medicine.* 2011;50(1):130-8.
- 19 26. Flagmeier P, De S, Wirthensohn DC, Lee SF, Vincke C, Muyldermans S, et al.
20 Ultrasensitive Measurement of Ca(2+) Influx into Lipid Vesicles Induced by Protein Aggregates.
21 *Angewandte Chemie (International ed in English).* 2017;56(27):7750-4.
- 22 27. Varela JA, Rodrigues M, De S, Flagmeier P, Gandhi S, Dobson CM, et al. Optical
23 Structural Analysis of Individual alpha-Synuclein Oligomers. *Angewandte Chemie (International*
24 *ed in English).* 2018;57(18):4886-90.
- 25 28. Lee JE, Sang JC, Rodrigues M, Carr AR, Horrocks MH, De S, et al. Mapping Surface
26 Hydrophobicity of alpha-Synuclein Oligomers at the Nanoscale. *Nano letters.* 2018;18(12):7494-
27 501.
- 28 29. De S, Wirthensohn DC, Flagmeier P, Hughes C, Aprile FA, Ruggeri FS, et al. Different
29 soluble aggregates of Abeta42 can give rise to cellular toxicity through different mechanisms.
30 *Nat Commun.* 2019;10(1):1541.
- 31 30. Drews A, De S, Flagmeier P, Wirthensohn DC, Chen WH, Whiten DR, et al. Inhibiting
32 the Ca(2+) Influx Induced by Human CSF. *Cell Rep.* 2017;21(11):3310-6.
- 33 31. Pavlov EV, Priault M, Pietkiewicz D, Cheng EH, Antonsson B, Manon S, et al. A novel,
34 high conductance channel of mitochondria linked to apoptosis in mammalian cells and Bax
35 expression in yeast. *J Cell Biol.* 2001;155(5):725-31.
- 36 32. Whiten DR, Zuo Y, Calo L, Choi ML, De S, Flagmeier P, et al. Nanoscopic
37 Characterisation of Individual Endogenous Protein Aggregates in Human Neuronal Cells.
38 *Chembiochem : a European journal of chemical biology.* 2018;19(19):2033-8.
- 39 33. Domijan AM, Kovac S, Abramov AY. Lipid peroxidation is essential for phospholipase C
40 activity and the inositol-trisphosphate-related Ca(2+)(+) signal. *Journal of cell science.*
41 2014;127(Pt 1):21-6.
- 42 34. Bengoa-Vergniory N, Roberts RF, Wade-Martins R, Alegre-Abarrategui J. Alpha-
43 synuclein oligomers: a new hope. *Acta Neuropathol.* 2017;134(6):819-38.
- 44 35. Masaracchia C, Hnida M, Gerhardt E, Lopes da Fonseca T, Villar-Pique A, Branco T, et
45 al. Membrane binding, internalization, and sorting of alpha-synuclein in the cell. *Acta*
46 *neuropathologica communications.* 2018;6(1):79.
- 47 36. Vaarmann A, Gandhi S, Abramov AY. Dopamine induces Ca²⁺ signaling in astrocytes
48 through reactive oxygen species generated by monoamine oxidase. *The Journal of biological*
49 *chemistry.* 2010;285(32):25018-23.

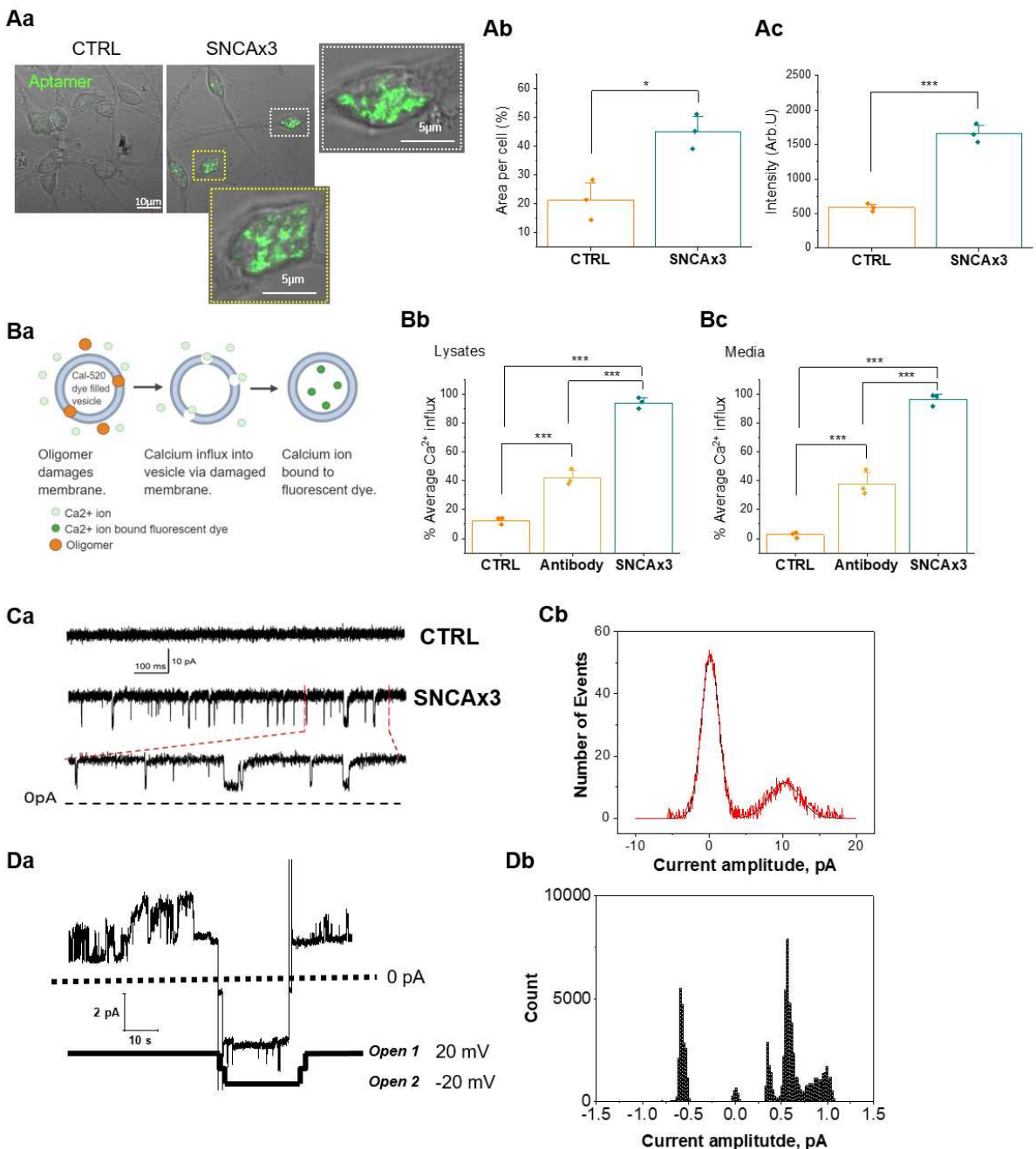
- 1 37. Vaarmann A, Gandhi S, Gourine AV, Abramov AY. Novel pathway for an old
2 neurotransmitter: dopamine-induced neuronal calcium signalling via receptor-independent
3 mechanisms. *Cell Calcium*. 2010;48(2-3):176-82.
- 4 38. Gandhi S, Abramov AY. Mechanism of oxidative stress in neurodegeneration. *Oxidative
5 medicine and cellular longevity*. 2012;2012:428010.
- 6 39. Dixon SJ, Lemberg KM, Lamprecht MR, Skouta R, Zaitsev EM, Gleason CE, et al.
7 Ferroptosis: an iron-dependent form of nonapoptotic cell death. *Cell*. 2012;149(5):1060-72.
- 8 40. Stockwell BR, Friedmann Angeli JP, Bayir H, Bush AI, Conrad M, Dixon SJ, et al.
9 Ferroptosis: A Regulated Cell Death Nexus Linking Metabolism, Redox Biology, and Disease.
10 *Cell*. 2017;171(2):273-85.
- 11 41. Kagan VE, Mao G, Qu F, Angeli JP, Doll S, Croix CS, et al. Oxidized arachidonic and
12 adrenic PEs navigate cells to ferroptosis. *Nature chemical biology*. 2017;13(1):81-90.
- 13 42. Agmon E, Solon J, Bassereau P, Stockwell BR. Modeling the effects of lipid peroxidation
14 during ferroptosis on membrane properties. *Sci Rep*. 2018;8(1):5155.
- 15 43. Lei P, Bai T, Sun Y. Mechanisms of Ferroptosis and Relations With Regulated Cell
16 Death: A Review. *Frontiers in physiology*. 2019;10:139.
- 17 44. Devos D, Moreau C, Devedjian JC, Kluza J, Petrault M, Laloux C, et al. Targeting
18 chelatable iron as a therapeutic modality in Parkinson's disease. *Antioxidants & redox signaling*.
19 2014;21(2):195-210.
- 20 45. Doll S, Proneth B, Tyurina YY, Panzilius E, Kobayashi S, Ingold I, et al. ACSL4 dictates
21 ferroptosis sensitivity by shaping cellular lipid composition. *Nature chemical biology*.
22 2017;13(1):91-8.
- 23 46. Martin-Bastida A, Ward RJ, Newbould R, Piccini P, Sharp D, Kabba C, et al. Brain iron
24 chelation by deferiprone in a phase 2 randomised double-blinded placebo controlled clinical trial
25 in Parkinson's disease. *Scientific reports*. 2017;7(1):1398.
- 26 47. Do Van B, Gouel F, Jonneaux A, Timmerman K, Gele P, Petrault M, et al. Ferroptosis, a
27 newly characterized form of cell death in Parkinson's disease that is regulated by PKC.
28 *Neurobiology of disease*. 2016;94:169-78.
- 29 48. Zaichick SV, McGrath KM, Caraveo G. The role of Ca(2+) signaling in Parkinson's
30 disease. *Dis Model Mech*. 2017;10(5):519-35.
- 31 49. Angelova PR, Horrocks MH, Klenerman D, Gandhi S, Abramov AY, Shchepinov MS.
32 Lipid peroxidation is essential for alpha-synuclein-induced cell death. *Journal of neurochemistry*.
33 2015;133(4):582-9.
- 34 50. Galvagnion C, Brown JW, Ouberai MM, Flagmeier P, Vendruscolo M, Buell AK, et al.
35 Chemical properties of lipids strongly affect the kinetics of the membrane-induced aggregation
36 of alpha-synuclein. *Proceedings of the National Academy of Sciences of the United States of
37 America*. 2016;113(26):7065-70.
- 38 51. Yang WS, Kim KJ, Gaschler MM, Patel M, Shchepinov MS, Stockwell BR. Peroxidation
39 of polyunsaturated fatty acids by lipoxygenases drives ferroptosis. *Proceedings of the National
40 Academy of Sciences of the United States of America*. 2016;113(34):E4966-75.
- 41 52. Narayan P, Holmstrom KM, Kim DH, Whitcomb DJ, Wilson MR, St George-Hyslop P, et
42 al. Rare individual amyloid-beta oligomers act on astrocytes to initiate neuronal damage.
43 *Biochemistry*. 2014;53(15):2442-53.
- 44 53. Imai H, Matsuoka M, Kumagai T, Sakamoto T, Koumura T. Lipid Peroxidation-
45 Dependent Cell Death Regulated by GPx4 and Ferroptosis. *Current topics in microbiology and
46 immunology*. 2017;403:143-70.
- 47 54. Schriever SC, Zimprich A, Pfuhlmann K, Baumann P, Giesert F, Klaus V, et al.
48 Alterations in neuronal control of body weight and anxiety behavior by glutathione peroxidase 4
49 deficiency. *Neuroscience*. 2017;357:241-54.

50



1
 2 **Figure 1. Abnormal calcium signalling in iPSC-derived neurons with SNCA x3.** A) Protocol to
 3 differentiate iPSC to cortical neurons. B) The majority of cells are Tuj 1 (and not GFAP-positive) in both
 4 control (CTRL) and mutant (SNCAx3) lines, Ba) Representative images with Tuj 1 (neuronal marker,
 5 red) and GFAP (astrocytic marker, green), DAPI (total cell number, blue). Bb) Percentage cell proportion
 6 expressing Tuj 1 or GFAP, N = 3 CTRL & SNCA. Ca) Representative tracers of cytosolic calcium rise in
 7 response to 5µM glutamate not to ATP. Cb) Percent GFAP cell population responding to either 5µM glutamate
 8 or 100µM ATP, N = 3 CTRL & SNCA. Cc) Application of 5µM glutamate induced a rise in cytosolic
 9 calcium, which was significantly higher in SNCA x3 neurons compared to control neurons, N = 3 CTRL
 10 & SNCA. Da) 5µM glutamate induces calcium signaling. Db) Depolarization of cells with 50mM KCl
 11 results in opening of voltage dependent calcium channels and a cytosolic calcium signal, which was

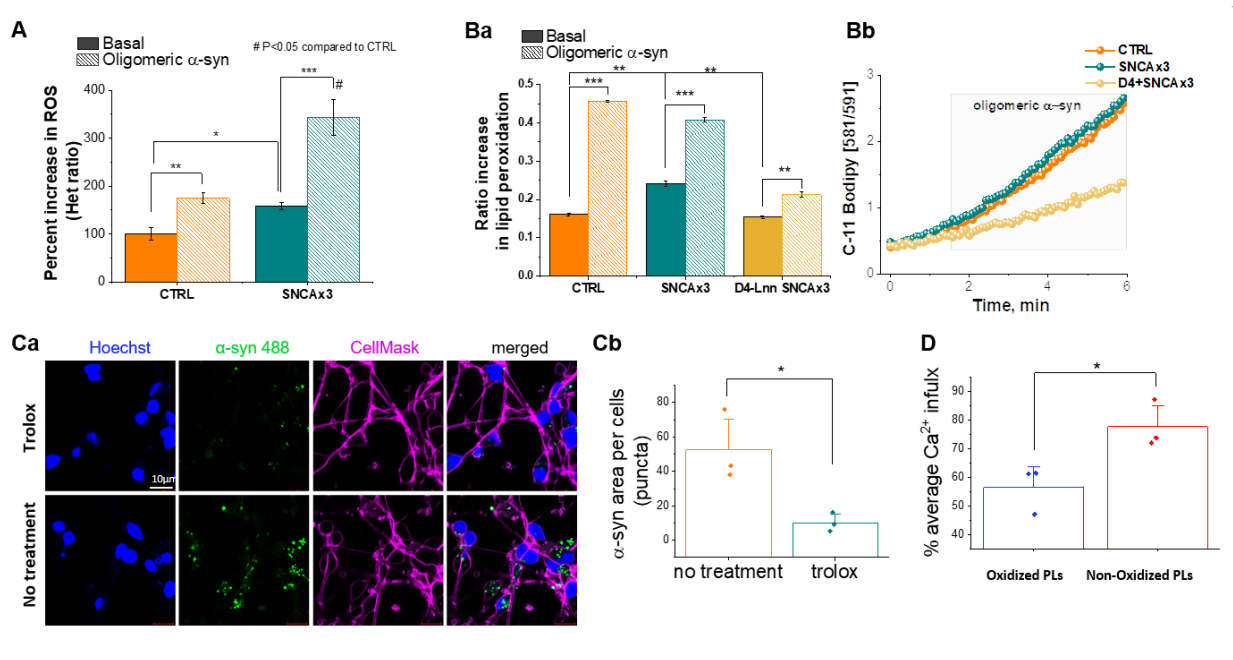
1 significantly higher in SNCA x3 neurons compared to control. Dc) Stimulation of the P2Y receptors with
 2 100uM ATP induced a cytosolic calcium signal that was significantly lower in the SNCA x3 cells
 3 compared to control. Dd) Histogram demonstrates the mean values of the calcium signals induced by
 4 glutamate, KCl and ATP (Mean \pm SEM), N = 3 per condition for CTRL & SNCA x3. Ea) Registered
 5 events of spiking activity in individual control and SNCA triplication cells (spikes are marked with
 6 arrows, orange-CTRL, teal-SNCA x3). Eb) No of events per cell*min*1000 (Mean \pm SEM). n = 180
 7 CTRL and 125 SNCA x3 cells. * $P < 0.05$, ** $P < 0.001$, *** $P < 0.0001$.



1 **Figure 2. α -synuclein aggregates disrupt membranes.** A) iPSC derived cortical neurons from patients
2 carrying 3x SNCA exhibit aggregates. Aa - c) Aptamer expression level (both area and intensity) is higher
3 in iPSC derived neurons with SNCA x3, N = 3 CTRL & SNCA x3. Ba) Illustration of membrane
4 permeabilization assay by measuring Ca^{2+} influx in vesicles. Bb & c) Cell lysates and media from
5 SNCAx3 induce higher level of permeabilization than control, prevented by antibody (phospho S129)
6 binding of α -synuclein aggregates, N = 3 CTRL & SNCA. Ca) Single-channel activity of α -synuclein in
7 the membrane of iPSC-derived neurons. Top: control recording from outside-out patch pulled from
8 control neurons. Middle: recording from outside-out patch pulled from SNCA x3 neurons. Bottom:
9 extended section of the medium trace marked by the dashed lines. Vertical scale bar applying to all three
10 traces; horizontal (time) scale bar apply to the top and medium trace. Cb) All-points amplitude histogram
11 of channel openings in the membrane of iPSC-derived neurons with SNCA3x, fitted with double-
12 Gaussian function, N = 3 CTRL & SNCA. Da) Single-channel activity of α -synuclein in the membrane of
13 giant liposomes consisting of lipids. Channels open followed by partial inactivation to a stable sub-
14 conductance level (open 1). After switch to -20 mV the channels open to a higher conductance state
15 (open 2). Db) Current amplitude histogram of the α -synuclein channel activity in giant liposome patch
16 represented in Ea. * $P < 0.05$, ** $P < 0.001$, *** $P < 0.0001$.

17

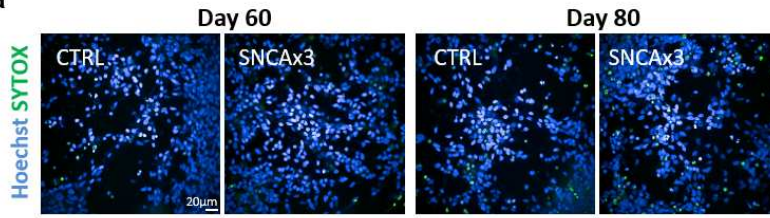
1



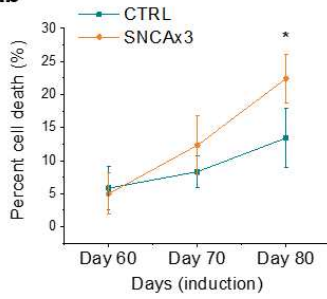
2

3 **Figure 3. ROS production and lipid peroxidation induced by α -synuclein in neurons.** A & B) SNCA
 4 3x neurons are vulnerable to exogenously applied α -synuclein oligomers A) Rate of ROS production in
 5 iPSC-derived SNCA x3 neurons is higher than in control neurons. (N = 3 CTRL, SNCA & D4-Lnn
 6 treated SNCA). Ba) Basal lipid peroxidation rate in iPSC-derived neurons with α -synuclein 3x is higher
 7 than the control neurons, but could be restored through pre-treatment with D4-Linolenic acid (D4-Lnn) in
 8 SNCA x3 neurons, which also prevented oligomer-induced lipid peroxidation (N = 3 CTRL, SNCA &
 9 D4-Lnn treated SNCA). Bb) Representative traces of Ba. C) Characterization of α -synuclein – membrane
 10 interactions. Ca) Representative images of exogenous oligomeric α -synuclein uptake (AF488
 11 fluorescence, green) into the cytoplasm (plasmic membranes are labelled with CellMaskTM Depp Red
 12 dye; magenta colour) in control neurons with or without Trolox treatment. Oligomer uptake was
 13 significantly reduced when membrane oxidation was inhibited by Trolox, N = 5 basal & Trolox. Cb)
 14 Trolox inhibits uptake of aggregate forms of α -synuclein. D) Calcium influx in the membrane
 15 permeabilisation assay was increased when vesicles composed of oxidised lipids were generated. 16:0 –
 16 20:4 PC non-oxidised membrane. Ox PAPC oxidised membrane, N = 3 non & oxidized membrane.
 17 * $P < 0.05$, ** $P < 0.001$, *** $P < 0.0001$.

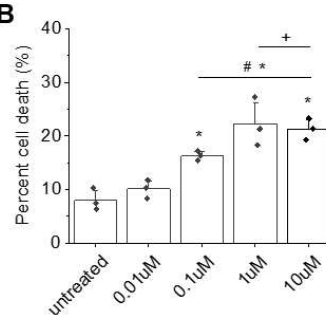
Aa



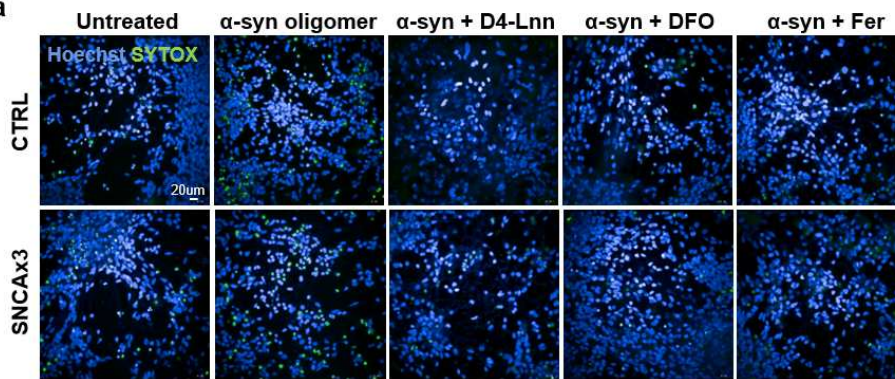
Ab



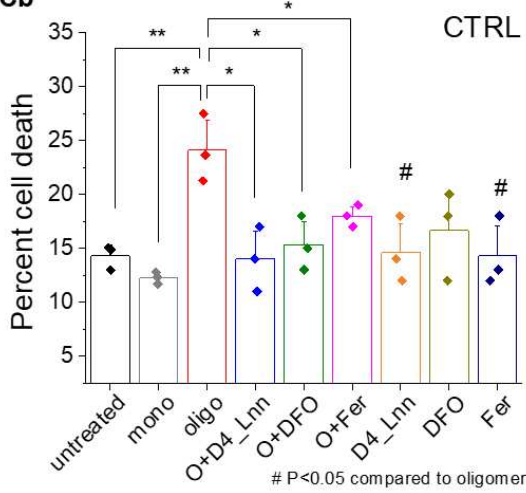
B



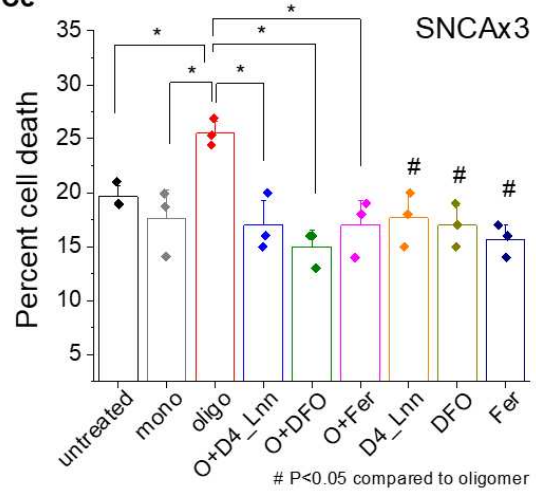
Ca



Cb

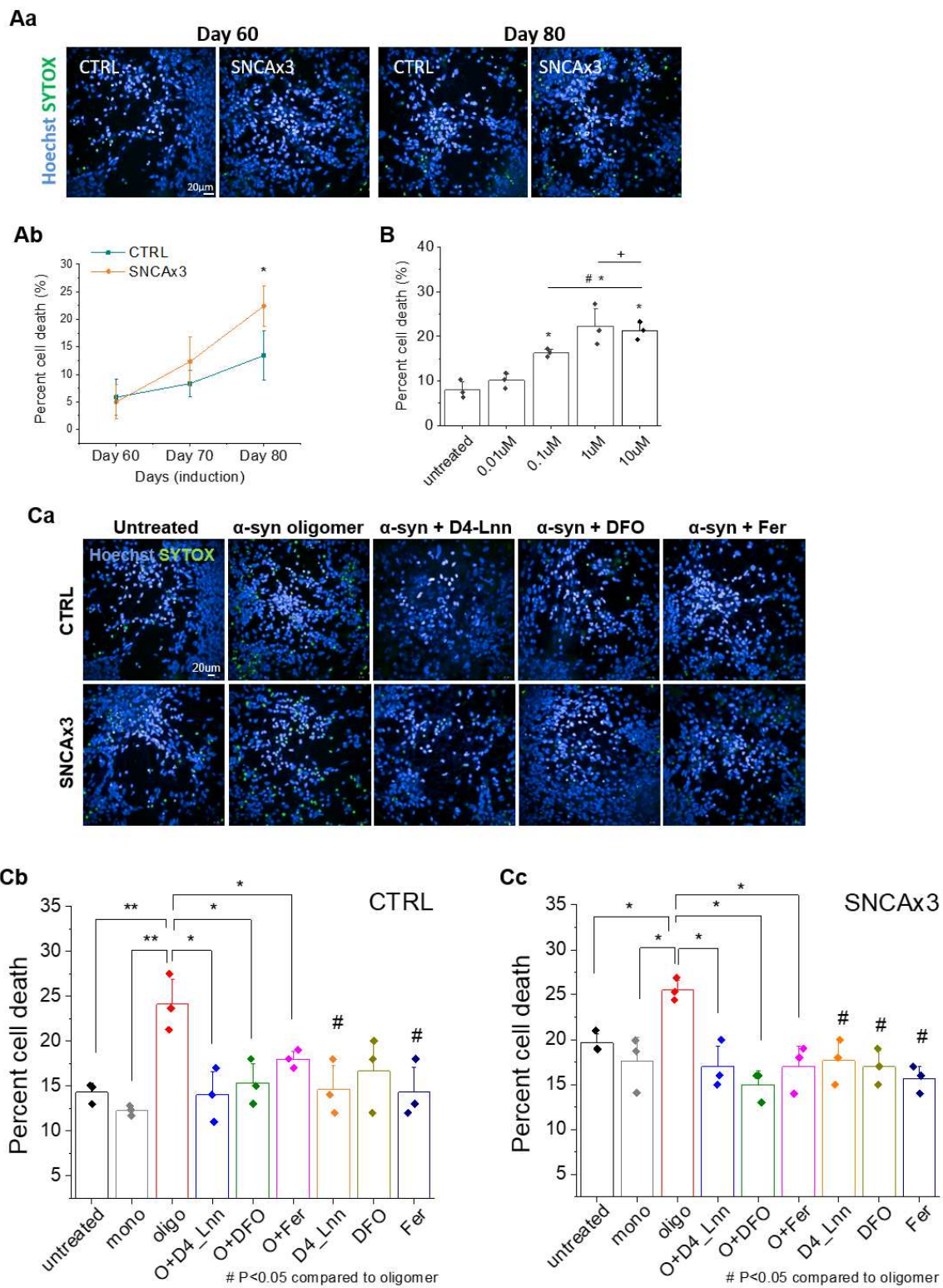


Cc



1 **Figure 4. Prevention of lipid peroxidation restores calcium dysregulation in SNCA 3x neurons.** A)
2 Representative traces showing deuterated PUFAs restore abnormal glutamate-induced calcium signaling
3 or KCl-induced depolarisation in SNCA x3 neurons (Ab) to control levels (Ac). B) ATP induced calcium
4 signal is smaller in the SNCA x3 cells (Bb) compared to control (Ba). This was also restored by pre-
5 incubation of the cells with D-PUFAs (Bc). C) Double bolus of dopamine (50µM) in SNCA x3 neurons
6 evoked dysregulated calcium signal (Cb) in comparison to control response (Ca). Cc) Pre-incubation of
7 the SNCA x3 cells with D4-Lnn prevents dopamine induced cytosolic calcium signals. D) Quantification
8 histograms depicting the preventive effect of deuterated PUFAs (D4-Lnn) on the calcium response to
9 application of glutamate (a, N = 4 CTRL, N = 5 SNCA, N = 7 D4-Lnn treated SNCA), KCl (b, N = 5
10 CTRL, N = 7 SNCA, N = 4 D4-Lnn treated SNCA), ATP (c, N = 4 CTRL, SNCA & D4-Lnn treated
11 SNCA) or dopamine (d, N = 5 CTRL, N = 3 & 4 SNCA, N = 3 D4-Lnn treated SNCA) in both control
12 and iPSC-derived neurons with SNCA x3. * $P < 0.05$, ** $P < 0.001$, *** $P < 0.0001$.

13

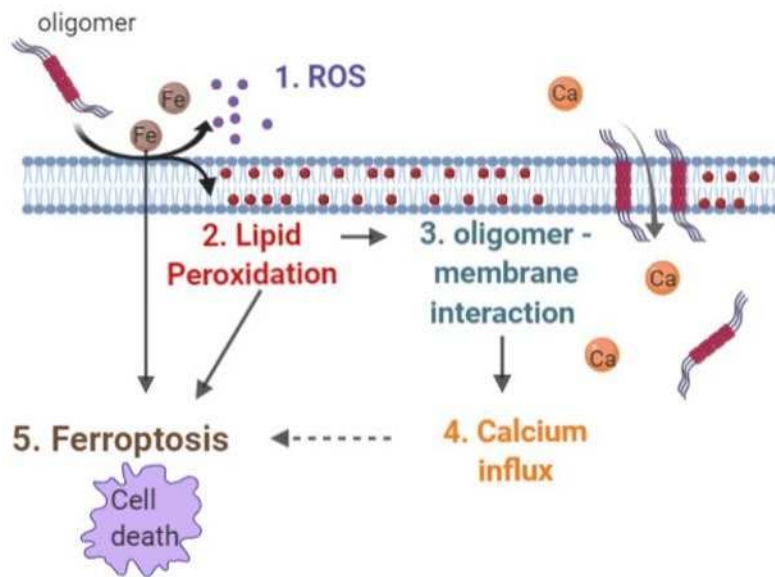


1
2

Figure 5. Increased cell death rate in SNCA x3 neurons is dependent on lipid peroxidation and on

1 **the presence of iron.** A) Cell viability of iPSC derived neurons over time in culture. Aa) Upon
2 completion of neuronal maturation > day 60 (22), SNCAx3 cells show similar cell viability with CTRL.
3 Neuronal loss of SNCA x3 is significantly increased over the following 20 days. Ab) Representative
4 images of cell death. B) A dose response (0.01 μ M – 10 μ M) effect of Erastin, a ferroptosis inducer, on
5 toxicity in iPSC derived cortical neurons. 100uM Erastin data was excluded due to the high toxicity
6 preventing accurate quantification of cell death (* $P < 0.05$ compared to untreated, # $P < 0.05$ compared
7 to 0.01 μ M and + $P < 0.05$ compared to 0.1 μ M condition. * $P < 0.05$, # $P < 0.05$ compared to untreated,
8 + $P < 0.05$ compared to 0.01 μ M). Ca) Representative images depicting α -synuclein-induced toxicity
9 induced by 1 μ M α -synuclein monomer (10nM oligomer) overnight and its rescue by blocking ferroptosis.
10 D-PUFA (48hr), Ferrostatin (1hr) & DFO (1hr) were pre-incubated prior to oligomer treatment). Blue-
11 Hoechst 33342 (total number of cells); green-SYTOX green (dead cells). Cb & c) Comparison of the
12 effects of transition metal ion chelator (DFO), inhibitor of lipid peroxidation (D4-Lnn), and Fer
13 (ferrostatin-1) a ferroptosis inhibitor on cell death, induced by α -synuclein oligomers within control (B, N
14 = 3 per condition) and SNCA triplication (C, N = 3 per condition). * $P < 0.05$, ** $P < 0.001$, *** $P < 0.0001$.

15



1

2 **Figure 6. Schematic diagram illustrating mechanisms of α -synuclein induced ferroptosis.**

3 Oligomeric α -synuclein induces 1) ROS and 2) lipid peroxidation within the membrane which results in

4 an increase in 3) oligomer – membrane interaction, and consequently causes 4) calcium influx. The

5 consequence of those events leads to cell death, 5) “Ferroptosis”.

6

7

8

9